coatings

MDPI

Article

N-Doped Carbon Nanoparticles as Antibacterial Agents on *Escherichia coli*: The Role of the Size and Chemical Composition of Nanoparticles

David Lopez-Diaz [1,*], María Dolores Merchán [1,2,*], Pilar Pérez [3] and María Mercedes Velázquez [1,2]

[1] Departamento de Química Física, Facultad de Ciencias Químicas, Universidad de Salamanca, 37008 Salamanca, Spain; mvsal@usal.es
[2] Laboratorio of Nanoelectronica and Nanomateriales, USAL-NANOLAB, Universidad de Salamanca, 37008 Salamanca, Spain
[3] Instituto de Biología Funcional y Genómica, CSIC, Universidad de Salamanca, 37007 Salamanca, Spain; piper@usal.es
* Correspondence: authors: dld@usal.es (D.L.-D.); mdm@usal.es (M.D.M.)

Abstract: In the last years N-doped carbon nanoparticles have been shown to have improved antibacterial activity over the undoped nanomaterial, but it is difficult to find correlations between the structure of the nanoparticle and its antibacterial activity. This prevents us from proposing a clear antibacterial mechanism and makes it difficult to select materials with the best physical and chemical properties for use as antibacterial agents. With this purpose, here, we analyze the effect of, the size and the surface chemical composition of four N-doped carbon nanoparticles on the growth of *Escherichia coli* bacteria, used in this work as a model of Gram-negative bacteria. Our results indicated great antibacterial activity as the concentration of the carbon nanoparticles increased. The IC50 values obtained ranged between 23 and 34 μg/mL, the lowest values found in the literature for CNPs in the absence of metals. The reduction rate was analyzed using a Ligand-Substrate model based on Monod's equation, which allows us to interpret the dependence of the nanoparticle-bacteria affinity with the nanomaterial structure. The results of the model indicate the contribution of two mechanisms, oxidative stress and the nanoknife in the antibacterial process on *Escherichia coli* bacteria.

Keywords: N-doped graphene carbon nanoparticles; antibacterial ability; *Escherichia coli*

check for updates

Citation: Lopez-Diaz, D.; Merchán, M.D.; Pérez, P.; Velázquez, M.M. N-Doped Carbon Nanoparticles as Antibacterial Agents on *Escherichia coli*: The Role of the Size and Chemical Composition of Nanoparticles. *Coatings* **2023**, *13*, 1169. https://doi.org/10.3390/coatings13071169

Academic Editors: Ajay Vikram Singh and Maria Cristina Tanzi

Received: 12 May 2023
Revised: 2 June 2023
Accepted: 25 June 2023
Published: 28 June 2023

1. Introduction

Due to the rapid and continuous increase of the world population, increasing air and water pollution are causing infectious diseases and pathogens to grow [1–4]. Likewise, the growth and adhesion of bacteria is a problem that causes a high cost in public health systems and in various industries such as clothing, biomedicine, food packaging, water treatment, and filtration [5,6]. The abuse of antibiotics such as fluoroquinolones, chloramphenicol, trimethoprim, and various carbapenem and β-lactam antibiotics, has made that many bacteria become drug resistant [7–10]. It has been proved that the mechanism of resistance in Gram-negative bacteria, such as *Escherichia coli* (*E. coli*), is based on restricting the entry of antibiotics into the cell through the outer membrane [1,11]. Therefore, the design of new biocompatible materials as substitutes of antibiotics is still a challenge.

Some metals such as Ag, Au and Pt [10,12–15], as well as metal oxides (CuO, Fe_2O_3, ZnO) [16–19] or hybrid compounds formed by metal oxides doped with a second metal (Mo/NiO) [20] or even nanoparticles made up of three metal oxides (CuO/ZnO/MnO_2) [21] present high antibacterial activity and have been successfully used as a coating in the prevention of biofouling [14,15,22,23] and in cancer therapy treatments [14]. The main drawback of these nanoparticles is their moderate chemical stability, which can lead to high toxicity due to the release of metal ions [13,24,25]. Therefore, it is necessary to find new materials of reduced toxicity.

An alternative to metallic materials raised in recent years is carbonaceous nanomaterials in different allotropic forms, such as fullerenes, carbon nanotubes (CNTs), especially single-walled carbon nanotubes (SWCNT), and graphene oxide (GO). These materials proved to be potential bactericidal agents [26] with low toxicity and for this reason are being widely tested for their use in medicine, as drug carriers, as a means for gene transport, or in tissue engineering [9,27–33]. Specifically, many review articles have emerged dedicated to exploring the therapeutic applications of Carbon Nanoparticles (CNPs), including graphene (G), graphene oxide (GO), and reduced graphene oxide (rGO) [30,32–35]. The different works have verified that carbonaceous nanoparticles (CNPs) cause membrane damage in bacteria by contact and aggregation between bacterial cells and carbon nanomaterials which lead to cell death [36,37] and have established that the antibacterial activity of the nanoparticles depends on their chemical composition as well as the thickness, size, and surface area [38,39]. CNPs, present different physicochemical properties due to the distinct oxidation degree and particle size that are well suited to limit microbial infection [1,2,6,9,29,30,32,40,41]. Despite the great variety of works related to the bacterial activity of carbonaceous materials isolated [42–44], or combined with metals and metal oxides [2,6,9,45–53] there is still work to be conducted if it is desired to avoid the presence of metals and the use of UV-Vis radiation, as well as to understand the relationship between physicochemical characteristics such as the size, chemical composition or morphology of CNPs and the antibacterial mechanism.

It was reported that when CNPs are in contact with bacterial cells, they can be destroyed by different mechanisms. The most accepted mechanisms are sharp edge cutting (nanoknife), oxidative stress by production of reactive oxygen species (ROS), and cell trapping (wrapping). When the CNPs act through a trapping mechanism, the bacterial cells are wrapped, remaining isolated from the external environment. The isolation restrings the access to nutrients killing the cells. This mechanism was reported for large nanoparticle size (>10 μm) because they have high adsorption capacity due to their higher surface energy and flexibility. Accordingly, large GO sheets demonstrated greater antimicrobial activity towards *E. coli* than the smaller ones [54,55]. In addition, the cell trapping mechanism is also influenced by the amphipathic properties of the CNPs, since nanomaterial-bacteria adhesion plays an important role in the ability to wrap the bacteria [54]. The size of the thinner and bigger CNPs have a complex effect on the antibacterial capacity, since they affect not only the wrapping ability but also the ability to destroy the cells through sharp edge-cutting effects. These mechanisms were observed when CNPs interact with the cell wall of different bacteria, such as *E. coli* and *S. aureus*, carcinoma cells, and normal mammalian cells [9,27,30,32,54–56].

The third mechanism responsible for bacterial death is oxidative stress [30,57]. The mechanism is related to a process of charge transfer between the CNPs and the different functional groups of the cell wall [54]. This charge-transfer process arises from the imbalance between the antioxidant and oxidation processes that finally kills the bacteria [58]. The mechanism is affected by the presence of electronegative functional groups to induce charge transfer when the nanomaterial is photoirradiated [43] causing the generation of ROS [40]. This mechanism is affected by the degree of functionalization of the material [1], but its size and surface curvature [59] have a significant influence on the effectiveness of the charge transfer process. Oxidative stress mechanism has satisfactorily been used to explain the antibacterial activity of metal oxide nanoparticles against Gram-positive and Gram-negative bacteria [20].

The results previously reported indicated that, the antibacterial mechanisms of CNPs can act either individually or simultaneously and that the predominant mechanism in each case must be related to the structure of the material, the surface chemical composition and size, however, this is an issue that still needs to be clarified since there are no studies in which these variables are systematically compared with the results of antibacterial activity.

The functionalization, the size of the particles, and the oxidation degree are highly dependent on the experimental conditions of the synthesis and on the starting materials used

as precursors [60–64]. Based on our previous experience in preparing and characterizing CNPs, the main objective of this work is to analyze the effect of the chemical composition and size on the antibacterial activity of CNPs against the Gram-negative bacteria *Escheriquia coli*. Our purpose is to demonstrate the antibacterial activity of N-doped carbon nanoparticles, without the presence of metals, and to delve into the physicochemical bases of bacteria-nanoparticle interactions.

To the best of our knowledge, this is the first time in the literature that Monod's model has been used to study the antibacterial capacity of CNPs as ligands. With this purpose, we have selected N-doped carbon nanoparticles synthesized from four different carbon precursors using acid oxidative synthesis, since we have proved in a previous work that both, size and chemical composition, depends on the precursors [65]. In particular, we have shown that the type of C-N bonds strongly depends on the precursor material used in the synthesis, and since that, the ability to donate electrons depends significantly on the type of C-N bond. Using this strategy we expect to deepen the physicochemical bases underlying the bacteria-nanoparticle interactions, facilitating the design of antibacterial agents based on carbon compounds.

2. Materials and Methods

2.1. Materials and Reagents

To modulate the size and chemical composition of carbon nanoparticles, CNPs, four starting materials were selected: three commercial graphite samples and one helical carbon nanofibers. The graphite samples were natural graphite flakes, 99.02 C fixed, supplied by Qingdao super graphite Co., Ltd. (Qingdao, China); and graphite powder of <20-micron particle size and highly oriented pyrolytic graphite (HOPG) supplied by Sigma Aldrich (St. Louis, MO, USA). Non-graphitized GANF® helical ribbon carbon nanofibers have been gifted by Carbon Advanced Materials, Grupo Antolín (Burgos, Spain). GANF® are synthesized by CVD using the floating catalyst method [66].

Reagents HNO_3 (65%), H_2SO_4 (98%), Na_2CO_3, and HCl (35%) were provided by Sigma Aldrich (St. Louis, MO, USA) and used without further purification.

To select a given size of the nanoparticles, a Spectra/Por® 6 Standard RC 2 kDa dialysis bag supplied by Spectrum Labs (San Francisco, CA, USA) was used. To prepare solutions and reagents for oxidation, ultrapure water prepared with a combination of Millipore's RiOs and Milli-Q systems was used. The conductivity of the water was less than 0.2 µS/cm and its surface tension value was 72.5 mNm^{-1}.

2.2. Synthesis of CNPs

CNPs were synthesized using the acidic oxidative process previously reported [65,67]. Briefly, 0.30 g of the graphitic materials were dispersed into a mixture of H_2SO_4 (60 mL) and HNO_3 (20 mL). To obtain a homogeneous solution, the mixtures were sonicated for two hours and further stirred for 24 h at 100 °C. Then, the brown solution becomes transparent since the graphitic material is completely dissolved.

The transparent solution was cooled at room temperature and diluted with MilliQ ultra-pure water (800 mL). The pH was adjusted to 8 by adding Na_2CO_3 and the color of the solutions changed from brown to light yellow. Finally, the solutions were filtered and further dialyzed for 3 days in a dialysis bag (retained molecular weight: 2 k Da). The list of acronyms corresponding to each precursor material can be found in the abbreviation list. The concentrations of aqueous solutions after dialysis were 0.45 (CNPNF) mg/mL, 0.28 (CNPPW) mg/mL, 0.21 (CNPHPG) mg/mL and 0.44 (CNPG) mg/mL.

2.3. Transmission Electron Microscopy (TEM)

Transmission electron microscopy (TEM) images were taken with a 120 kV Tecnai G2 Spirit TWIN from FEI (Hillsboro, OR, USA). The line resolution is 0.2 nm. Materials were deposited by the drop casting method on a holey carbon grid, HC200–Cu Holey Carbon (200 mesh) from Embra Grids. The particle size was calculated from TEM images of films

using the free ImageJ free software (version 153, 2023, Wisconsin University, Madison, WI, USA).

2.4. Antibacterial Test

The antibacterial activity of the CNPs was evaluated against the Gram-negative bacteria *Escherichia coli* (*E. coli* DH5α) following the methodology in reference [68] including slight modifications. Briefly, *E. coli* grown in Luria–Bertoni (LB) media was incubated at (10^{-6} bacteria/mL) with fresh solutions of CNPs for 1 h at 37 °C. The CNP concentrations in the LB medium varied between 10 and 60 μg/mL. Subsequently, the bacteria were diluted 100 times and aliquots containing about 125 bacteria were withdrawn and spread in 25 mL LB-agar plates. These plates were incubated at 37 °C for 24 h and then, the antibacterial activity was evaluated by colony counting method. The colonies were counted and compared with those on control plated without carbon nanoparticles, then, the antibacterial capacity was calculated in terms of reduction rate percentage from the following equation [5]

$$Reduction\ rate\ \% = \frac{N_{control} - N_{sample}}{N_{control}} \times 100 \quad (1)$$

In Equation (1) $N_{control}$ and N_{sample} represent the number of colonies from the control, without CNP, and for each CNP sample respectively as a function of the concentration. All treatments were prepared in duplicate and repeated at least three times for each sample and were conducted in the dark. Data in graphics represent the averaged values and the error bars are the standard deviations.

3. Results

N-CNPs were characterized by X-ray photoelectron spectroscopy (XPS) to determine their surface composition and transmission electron microscopy (TEM) and Tracking analysis (NTA) to obtain the nanoparticle's size. The surface atomic composition of *N* ranged from 0.4 and 1.6.

As can be observed in Figure 1, CNPs synthesized from different carbonaceous materials present different sizes and morphologies. Nanoparticles synthesized from carbon nanofibers (CNPNF, Figure 1a) are mainly constituted by small carbon dots of size close to 10 nm in diameter. These results are in agreement with previously published results in which a frequency analysis of the images was performed, showing single-mode distribution peaks with maximum frequencies centered at 10 nm in diameter [65]. For the rest of the materials, the TEM images show large and aggregated carbon nanoparticles formed during solvent evaporation and due to the hydrodynamic processes [69,70] (Figure 1b–d). To avoid this aggregation, we used Nanoparticle Tracking Analysis, NTA to obtain the diameter of the free nanoparticles [65]. The values obtained for the diameter of the four types of nanoparticles are collected in Table 1.

Table 1. Structural properties of N-CNPs.

Materials	Precursor	Diameter [1]/nm	Amine Groups [1] % (XPS)	Imine Groups [1] % (XPS)	K/μg^{-1} mL	Chi-Sqr
CNPNF	Carbon nanofibers	9.3 ± 0.9	47 ± 3	32 ± 3	0.043 ± 0.001	0.942
CNPPW	Graphite powder	93.6 ± 3.8	36 ± 3	22 ± 2	0.030 ± 0.002	0.955
CNPHPG	Pyrolytic graphite	52.0 ± 1	21 ± 2	16 ± 1	0.029 ± 0.003	0.967
CNPG	Graphite flakes	85.3 ± 1.1	35 ± 3	30 ± 3	0.032 ± 0.004	0.981

[1] Data from ref. [65].

To study the effect of the concentration on the bactericidal activity of CNPs, *E. coli* bacteria were incubated at 37 °C with different CNP concentrations in the range of 10 to 60 μg/mL for 1 h, and were spread in plates with LB-agar, for more details see Section 2.

Figure 2 shows that for the control experiment (C = 0 μg/mL), the number of colonies is similar in all the results obtained, indicating the robustness of the measurement protocol. It can also be seen that as the concentration of CNPs increases, a decrease in the number of *E. coli* colonies contained in the Petri dishes is observed, indicating a concentration dependency. Similar results have been observed for carbon [26] and metal oxide nanoparticles [21].

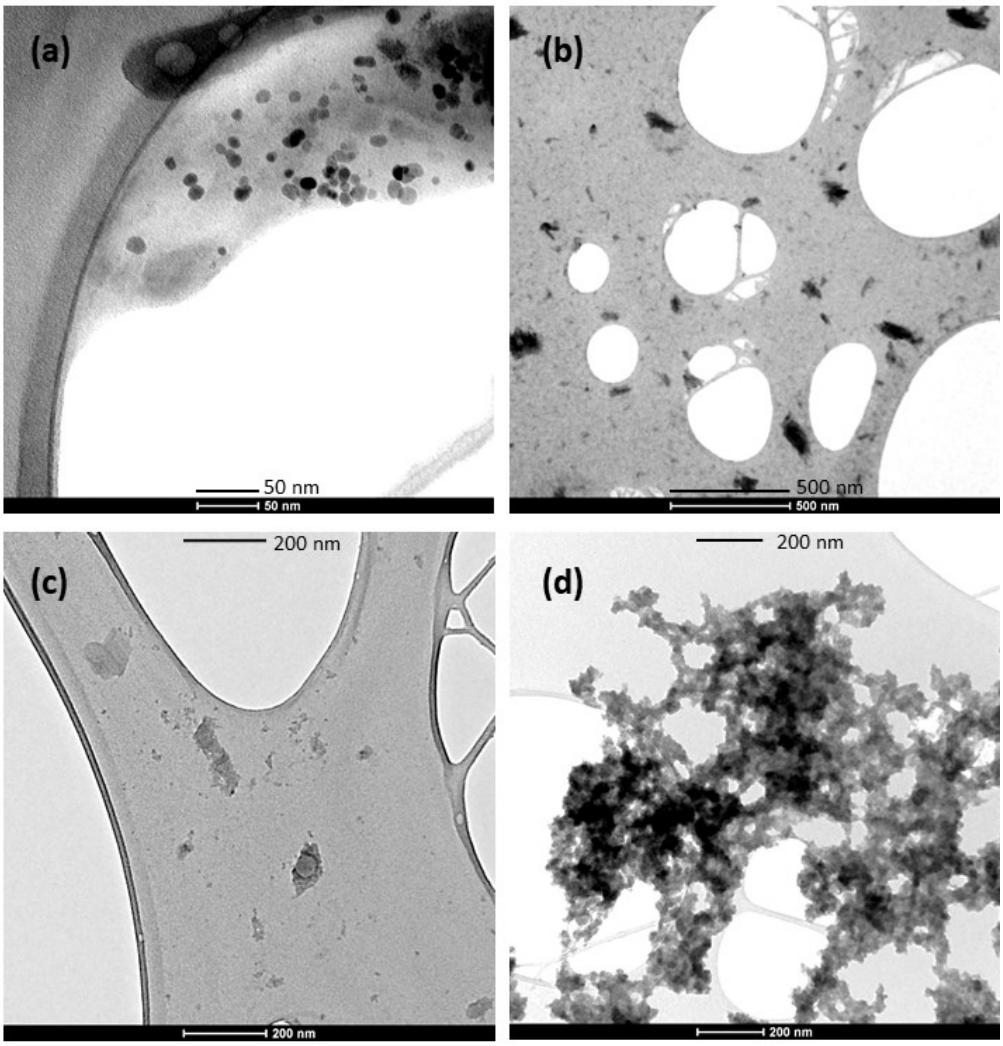

Figure 1. TEM images of CNPs obtained from different precursors. (**a**) CNPNF from carbon nanofibers, (**b**) CNPPW from graphite powder, (**c**) CNPHPG from pyrolytic graphite, and (**d**) CNPG from graphite flakes.

To study the dependence of the antibacterial activity on the concentration of nanoparticles, Figure 3 shows the evolution of the number of *E. coli* colonies with the concentration of nanomaterials. The number of colonies was obtained by the counting method. As a control, a plate without CNPs was prepared following the protocol described.

As shown in Figure 3, the number of colonies decreases with the concentration of nanoparticles while the rate of reduction clearly depends on the material. To quantify the differences between the samples, we calculated the percentage value of the reduction rate value using Equation (1), [5,71] and the values are plotted against the nanoparticle concentration in Figure 4.

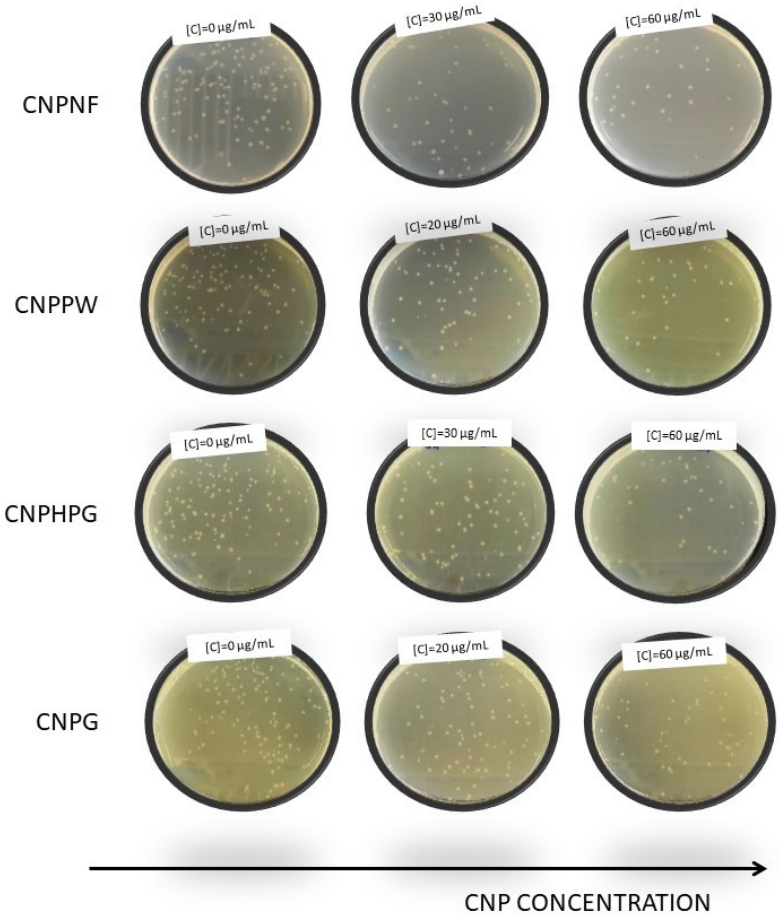

Figure 2. Evolution of the number of bacterial colonies with the concentration of CNPs for different Carbon Nanoparticles.

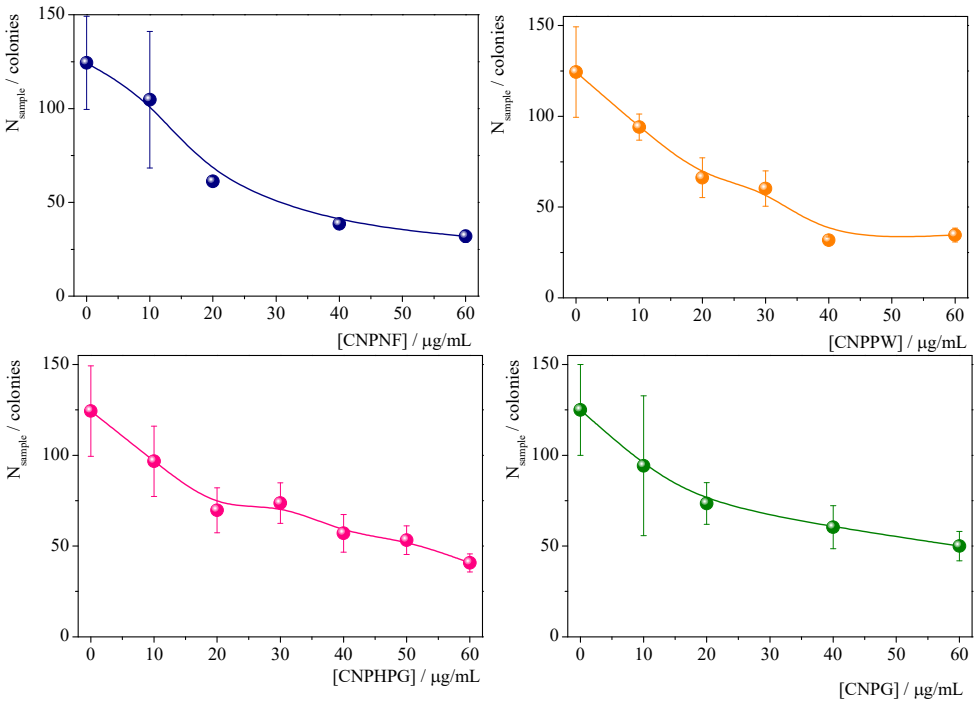

Figure 3. Evolution of the number of bacterial colonies with the concentration of CNPs. Error bars are calculated from the standard deviation of six different samples.

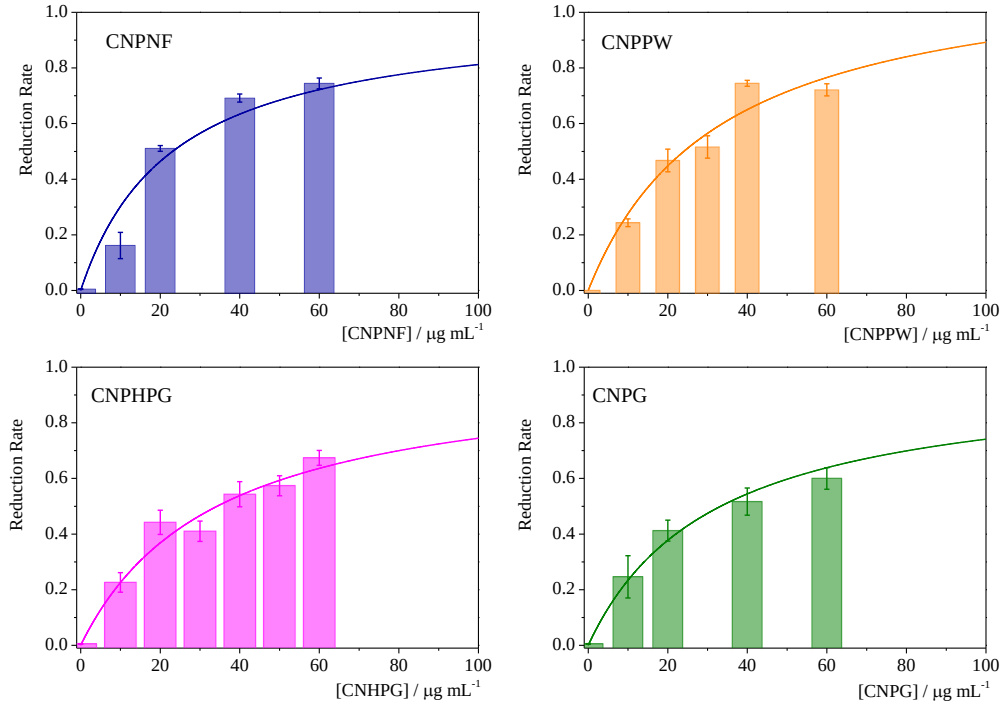

Figure 4. Variation of the antibacterial capacity as a function of the percentage values of the reduction rate, Equation (1), with the concentration of carbon nanoparticles. The lines represent the best fit of the reduction rate against the concentration of CNP according to Monod's model. Error bars are calculated from the standard deviation of six different samples.

4. Discussion

As can be seen in Figure 4, the antibacterial capacity increases with the concentration of nanoparticles up to saturation at a certain concentration of CNPs. However, the concentration dependence appears to be different for each material. We want to interpret this behavior from a physicochemical point of view and clarify the mechanisms that act between CNPs and bacteria. We assume that initially there must be an interaction between the chemical groups of the bacterial wall and the functional groups of the nanomaterials. Consequently, the formation rate of the Bacteria-nanoparticle complex (B-CNP) could be proportional to the reduction rate presented in Figure 4 and assume that if the B-CNP complex is formed, the result is the death of the bacteria. To model the formation of the complex, we assumed a reversible equilibrium between bacteria (B) and nanoparticles (CNP) and the bacteria-nanoparticle complex, [B-CNP].

$$\mathrm{B} + \mathrm{CNP} \leftrightarrow [\mathrm{B\text{-}CNP}]$$

This equilibrium is studied using a mathematical model based on Monod's equation in terms of the reduction rate of the colony, *RR* [72,73] by using Equation (2).

$$RR = \frac{RR_{max}[CNP]}{1/K + [CNP]} \tag{2}$$

The Monod's model relates the reduction rate, *RR* to the substrate concentration (*CNP*) which models the inhibition of bacterial growth through two parameters, the maximum specific reduction rate (RR_{max}), and the substrate affinity constant (*K*). Since the inhibition is similar to the enzyme activity model, the equation is similar to that described by the Michaelis-Menten model, and Equation (2) acquires a hyperbolic mathematical shape.

The results of the reduction rate (Figure 2) have been fitted to Monod's model (Equation (2)). The simulated curves have been also inserted in Figure 4 and parameters obtained from fits (*K* and Chi-sqr) are collected in Table 1. As can be seen in Figure 4, the model fits acceptably our experimental results. The value of RR_{max} has not been in-

cluded in Table 1 because the mathematical fit of the data assigns a value close to unity for all cases, taking into account the experimental error. This result would mean that the N-doped CNPs synthesized in this work have 100% efficiency as bactericides for *E. coli*. Similar efficiency values have been obtained for N-Doped Carbon Dots subjected to photoirradiation treatment over *E. coli* [43]. Without irradiation, efficiencies typically do not exceed 90% using carbon nanoparticles [42].

In Monod's model, $1/K$ represents the concentration at which 50% of the bacteria have been inhibited. Our results show $1/K$ values ranging between 23.3 and 34.5 μg/mL. This value can be compared with the same parameter obtained by other authors, who obtain IC50 between 550 and 700 μg/mL for carbon dots doped with N [42], or IC50 of 440 μg/mL for Carbon Quantum Dots obtained by hydrothermal synthesis [44]. Hybrid GO-CuO nanoparticles [52] were tested as an antibacterial agent against *E. coli*, and the IC50 was much higher, between 2–3 mg/mL. Lower IC50 values, 2–3 μg/mL have been found for *E. coli* antibacterial activity for GO and Ag hybrid materials [47,48].

Data in Figure 4 shows that the shape of the reduction rate curve, as well as the values of the affinity constant obtained from the fits, depend on the nanomaterial used as antibacterial agent. This means that the bactericidal activity could be related to the chemical composition and/or the size of the nanomaterial, among other factors. Other authors have pointed out this correlation, from a qualitative point of view, for fullerene [26,58] carbon nanotubes [26,59] or graphene oxide [26,74].

To check these issues, we have plotted in Figure 5 the affinity constant, K, against the sum of the percentage of amine and imine groups and against the diameter of the nanoparticles (data taken from Table 1). The results in Figure 5a indicate a correlation between the affinity constant and the sum of the percentage of amine and imine groups. This behavior is consistent with results previously reported in which it is assumed that N groups of the nanoparticle interact with the cell [75] through electron-transfer processes. Consequently, when the amine and imine groups in the material increase, the number of N atoms with non-bonding electrons also increases favoring the interactions between the material and the bacteria by electron charge mechanism. These electron transfer processes induce an alteration of the bacterial enzymes, the so-called oxidative stress mechanism [75].

It is interesting to note, that the bactericidal character of nanoparticles comes from the chemical interaction between the N-functional groups attached to the wall of the bacteria as was referenced previously [76]. The size of the nanoparticles would also be expected to play an important role in the reduction rate. In Figure 5b we can observe that the affinity constant decreases as the diameter of the nanoparticle increases. This indicates the existence of an additional antibacterial mechanism. According to the results in Figure 5b, a wrapping mechanism could be ruled out, since in that case, the bactericidal power, and consequently, the affinity constant, should increase with the size of the nanoparticles. Since the affinity constant decreases when the size of the nanoparticles increases, the behavior could be interpreted through the nanoknife mechanism acting simultaneously with the oxidative stress. Another interpretation could be to assume a steric hindrance that hinders the encounter between the reactive groups located in the bacteria wall and the N-groups of the nanomaterials [30].

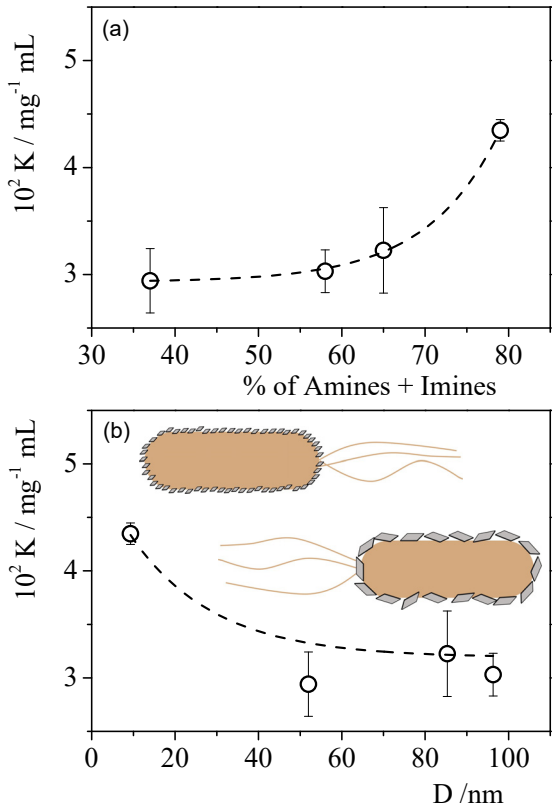

Figure 5. Evolution of the affinity constant, *K* with (**a**) the percentage of amines and imines, (**b**) the size of the *N*-doped nanoparticles. The dashed lines are visual guides. The error bars in *K* correspond to the standard deviation of the experimental data.

5. Conclusions

We have synthesized *N*-doped carbon nanoparticles as antibacterial agents using acid oxidative synthesis and four carbon precursors, resulting in nanomaterials with the different chemical compositions of *N*- and O-groups, and different diameters. Using these four materials, we have analyzed the influence of the surface chemical composition and the size of the materials on the antibacterial activity against *Escherichia coli* bacteria. Our results prove that the antibacterial activity increases as the concentration of nanoparticles increases. The behavior was modeled by Monod's equation considering the formation of a complex between the bacterial cell wall and the functional groups of the nanoparticles as responsible for the antibacterial activity. Given that the affinity constant calculated from the model increases with the presence of the amine and imine groups of the nanomaterials, it was possible to conclude that the mechanism of antibacterial activity may be due to electron transfer processes between the *N* groups of the nanomaterial and the functional groups of the bacteria, oxidative stress. Our results also point to the existence of an additional mechanism, probably nanoknife or steric hindrance, which acts simultaneously with oxidative stress.

The strength of the work lies in having prepared carbonaceous nanomaterials doped with *N* with antibacterial activity against *E. coli* bacteria without the need to introduce metals or irradiate with UV-vis, significantly reducing the risks of toxicity and the economic cost. As far as we know, the IC50 values are the lowest found in the literature for carbonaceous materials.

Author Contributions: Conceptualization, D.L.-D. and M.M.V.; methodology, P.P., D.L.-D. and M.M.V.; investigation, P.P., D.L.-D., M.D.M. and M.M.V.; data curation, D.L.-D., M.D.M. and M.M.V.; writing—original draft preparation, D.L.-D., M.D.M. and M.M.V.; writing—review and editing, D.L.-D., M.D.M., P.P. and M.M.V.; funding acquisition, M.M.V. All authors have read and agreed to the published version of the manuscript.

Funding: This research was funded by the European Regional Development Fund, ERDF, and Junta de Castilla y León grant number SA121P20 and MINECO, grants CTQ2016-78895-R and PGC2018-098924-B-100.

Institutional Review Board Statement: Not applicable.

Informed Consent Statement: Not applicable.

Data Availability Statement: Not applicable.

Acknowledgments: Authors thank García Fierro (Instituto de Catálisis y Petroleoquímica, Madrid) for XPS measurements.

Conflicts of Interest: The authors declare no conflict of interest.

Abbreviations

CNPNF	carbon nanoparticles synthesized from GANF carbon nanofibers (non-graphitized)
CNPPW	carbon nanoparticles synthesized from graphite powers
CNPHPG	carbon nanoparticles synthesized from Highly Oriented Pyrolytic Graphite
CNPG	carbon nanoparticles synthesized from graphite flakes
G	Graphene
GO	Graphene Oxide
rGO	Reduced Graphene Oxide
N-CNPs	N-doped carbon nanoparticles
CNPs	Carbon Nanoparticles
ROS	Reactive Oxidative Species
XPS	X-ray photoelectronic spectroscopy
TEM	Transmission electron microscopy
NTA	Nanoparticle tracking analysis

References

1. Anand, A.; Unnikrishnan, B.; Wei, S.-C.; Chou, C.P.; Zhang, L.-Z.; Huang, C.-C. Graphene oxide and carbon dots as broad-spectrum antimicrobial agents—a minireview. *Nanoscale Horiz.* **2019**, *4*, 117–137. [PubMed]
2. Fatima, N.; Qazi, U.Y.; Mansha, A.; Bhatti, I.A.; Javaid, R.; Abbas, Q.; Nadeem, N.; Rehan, Z.A.; Noreen, S.; Zahid, M. Recent developments for antimicrobial applications of graphene-based polymeric composites: A review. *J. Ind. Eng. Chem.* **2021**, *100*, 40–58.
3. Dong, A.; Wang, Y.-J.; Gao, Y.; Gao, T.; Gao, G. Chemical Insights into Antibacterial N-Halamines. *Chem. Rev.* **2017**, *117*, 4806–4862. [PubMed]
4. Zhang, X.; Kong, H.; Yang, G.; Zhu, D.; Luan, X.; He, P.; Wei, G. Graphene-Based Functional Hybrid Membranes for Antimicrobial Applications: A Review. *Appl. Sci.* **2022**, *12*, 4834. [CrossRef]
5. Díez-Pascual, A.M. Antibacterial Activity of Nanomaterials. *Nanomaterials* **2018**, *8*, 359. [CrossRef]
6. Díez-Pascual, A.M. Antibacterial Action of Nanoparticle Loaded Nanocomposites Based on Graphene and Its Derivatives: A Mini-Review. *Int. J. Mol. Sci.* **2020**, *21*, 3563.
7. Fair, R.J.; Tor, Y. Antibiotics and Bacterial Resistance in the 21st Century. *Perspect. Med. Chem.* **2014**, *6*, S14459.
8. Kavanagh, K.T.; Calderon, L.E.; Saman, D.M.; Abusalem, S.K. The use of surveillance and preventative measures for methicillin-resistant *Staphylococcus aureus* infections in surgical patients. *Antimicrob. Resist. Infect. Control* **2014**, *3*, 18. [CrossRef]
9. Ji, H.; Sun, H.; Qu, X. Antibacterial applications of graphene-based nanomaterials: Recent achievements and challenges. *Adv. Drug Deliv. Rev.* **2016**, *105*, 176–189.
10. Zheng, K.; Setyawati, M.I.; Leong, D.T.; Xie, J. Antimicrobial Gold Nanoclusters. *ACS Nano* **2017**, *11*, 6904–6910. [CrossRef]
11. Miller, S.I. Antibiotic Resistance and Regulation of the Gram-Negative Bacterial Outer Membrane Barrier by Host Innate Immune Molecules. *mBio* **2016**, *7*, e01541-16. [CrossRef] [PubMed]
12. Hoseinnejad, M.; Jafari, S.M.; Katouzian, I. Inorganic and metal nanoparticles and their antimicrobial activity in food packaging applications. *Crit. Rev. Microbiol.* **2018**, *44*, 161–181. [PubMed]
13. Zheng, K.; Setyawati, M.I.; Leong, D.T.; Xie, J. Surface Ligand Chemistry of Gold Nanoclusters Determines Their Antimicrobial Ability. *Chem. Mater.* **2018**, *30*, 2800–2808. [CrossRef]

14. Majumdar, M.; Biswas, S.C.; Choudhury, R.; Upadhyay, P.; Adhikary, A.; Roy, D.N.; Misra, T.K. Synthesis of Gold Nanoparticles Using Citrus macroptera Fruit Extract: Anti-Biofilm and Anticancer Activity. *ChemistrySelect* **2019**, *4*, 5714–5723.
15. Majumdar, M.; Khan, S.A.; Nandi, N.B.; Roy, S.; Panja, A.S.; Roy, D.N.; Misra, T.K. Green Synthesis of Iron Nanoparticles for Investigation of Biofilm Inhibition Property. *ChemistrySelect* **2020**, *5*, 13575–13583. [CrossRef]
16. Raghunath, A.; Perumal, E. Metal oxide nanoparticles as antimicrobial agents: A promise for the future. *Int. J. Antimicrob. Agents* **2017**, *49*, 137–152.
17. Sirelkhatim, A.; Mahmud, S.; Seeni, A.; Kaus, N.H.M.; Ann, L.C.; Bakhori, S.K.M.; Hasan, H.; Mohamad, D. Review on Zinc Oxide Nanoparticles: Antibacterial Activity and Toxicity Mechanism. *Nano-Micro Lett.* **2015**, *7*, 219–242.
18. Liu, J.; Wang, Y.; Ma, J.; Peng, Y.; Wang, A. A review on bidirectional analogies between the photocatalysis and antibacterial properties of ZnO. *J. Alloy. Compd.* **2019**, *783*, 898–918.
19. Chankhanittha, T.; Nanan, S. Visible-light-driven photocatalytic degradation of ofloxacin (OFL) antibiotic and Rhodamine B (RhB) dye by solvothermally grown ZnO/Bi_2MoO_6 heterojunction. *J. Colloid Interface Sci.* **2021**, *582*, 412–427.
20. Alam, M.W.; BaQais, A.; Mir, T.A.; Nahvi, I.; Zaidi, N.; Yasin, A. Effect of Mo doping in NiO nanoparticles for structural modification and its efficiency for antioxidant, antibacterial applications. *Sci. Rep.* **2023**, *13*, 1328.
21. Alam, M.W.; Al Qahtani, H.S.; Souayeh, B.; Ahmed, W.; Albalawi, H.; Farhan, M.; Abuzir, A.; Naeem, S. Novel Copper-Zinc-Manganese Ternary Metal Oxide Nanocomposite as Heterogeneous Catalyst for Glucose Sensor and Antibacterial Activity. *Antioxidants* **2022**, *11*, 1064. [CrossRef] [PubMed]
22. Liu, Z.; Zheng, X.; Zhang, H.; Li, W.; Jiang, R.; Zhou, X. Review on formation of biofouling in the marine environment and functionalization of new marine antifouling coatings. *J. Mater. Sci.* **2022**, *57*, 18221–18242.
23. Majumdar, M.; Khan, S.A.; Biswas, S.C.; Roy, D.N.; Panja, A.S.; Misra, T.K. In vitro and in silico investigation of anti-biofilm activity of *Citrus macroptera* fruit extract mediated silver nanoparticles. *J. Mol. Liq.* **2020**, *302*, 112586.
24. Wang, D.; Lin, Z.; Wang, T.; Yao, Z.; Qin, M.; Zheng, S.; Lu, W. Where does the toxicity of metal oxide nanoparticles come from: The nanoparticles, the ions, or a combination of both? *J. Hazard. Mater.* **2016**, *308*, 328–334.
25. Soenen, S.J.; Parak, W.J.; Rejman, J.; Manshian, B. (Intra)Cellular Stability of Inorganic Nanoparticles: Effects on Cytotoxicity, Particle Functionality, and Biomedical Applications. *Chem. Rev.* **2015**, *115*, 2109–2135.
26. Maleki Dizaj, S.; Mennati, A.; Jafari, S.; Khezri, K.; Adibkia, K. Antimicrobial Activity of Carbon-Based Nanoparticles. *Adv. Pharm. Bull.* **2015**, *5*, 19–23.
27. Tu, Y.; Lv, M.; Xiu, P.; Huynh, T.; Zhang, M.; Castelli, M.; Liu, Z.; Huang, Q.; Fan, C.; Fang, H.; et al. Destructive extraction of phospholipids from *Escherichia coli* membranes by graphene nanosheets. *Nat. Nanotechnol.* **2013**, *8*, 594–601. [CrossRef]
28. Bitounis, D.; Ali-Boucetta, H.; Hong, B.H.; Min, D.-H.; Kostarelos, K. Prospects and Challenges of Graphene in Biomedical Applications. *Adv. Mater.* **2013**, *25*, 2258–2268.
29. Shi, L.; Chen, J.; Teng, L.; Wang, L.; Zhu, G.; Liu, S.; Luo, Z.; Shi, X.; Wang, Y.; Ren, L. The Antibacterial Applications of Graphene and Its Derivatives. *Small* **2016**, *12*, 4165–4184.
30. Zou, X.; Zhang, L.; Wang, Z.; Luo, Y. Mechanisms of the Antimicrobial Activities of Graphene Materials. *J. Am. Chem. Soc.* **2016**, *138*, 2064–2077.
31. Jian, H.-J.; Wu, R.-S.; Lin, T.-Y.; Li, Y.-J.; Lin, H.-J.; Harroun, S.G.; Lai, J.-Y.; Huang, C.-C. Super-Cationic Carbon Quantum Dots Synthesized from Spermidine as an Eye Drop Formulation for Topical Treatment of Bacterial Keratitis. *ACS Nano* **2017**, *11*, 6703–6716.
32. Xin, Q.; Shah, H.; Nawaz, A.; Xie, W.; Akram, M.Z.; Batool, A.; Tian, L.; Jan, S.U.; Boddula, R.; Guo, B.; et al. Antibacterial Carbon-Based Nanomaterials. *Adv. Mater.* **2019**, *31*, 1804838.
33. Raul, P.K.; Thakuria, A.; Das, B.; Devi, R.R.; Tiwari, G.; Yellappa, C.; Kamboj, D.V. Carbon Nanostructures as Antibacterials and Active Food-Packaging Materials: A Review. *ACS Omega* **2022**, *7*, 11555–11559.
34. Hu, W.; Peng, C.; Luo, W.; Lv, M.; Li, X.; Li, D.; Huang, Q.; Fan, C. Graphene-Based Antibacterial Paper. *ACS Nano* **2010**, *4*, 4317–4323. [PubMed]
35. Krishnamoorthy, K.; Veerapandian, M.; Yun, K.; Kim, S.J. The chemical and structural analysis of graphene oxide with different degrees of oxidation. *Carbon* **2013**, *53*, 38–49. [CrossRef]
36. Kang, S.; Pinault, M.; Pfefferle, L.D.; Elimelech, M. Single-Walled Carbon Nanotubes Exhibit Strong Antimicrobial Activity. *Langmuir* **2007**, *23*, 8670–8673. [CrossRef] [PubMed]
37. Murray, A.R.; Kisin, E.R.; Tkach, A.V.; Yanamala, N.; Mercer, R.; Young, S.-H.; Fadeel, B.; Kagan, V.E.; Shvedova, A.A. Factoring-in agglomeration of carbon nanotubes and nanofibers for better prediction of their toxicity versus asbestos. *Part. Fibre Toxicol.* **2012**, *9*, 10.
38. Hajipour, M.J.; Fromm, K.M.; Akbar Ashkarran, A.; Jimenez de Aberasturi, D.; de Larramendi, I.R.; Rojo, T.; Serpooshan, V.; Parak, W.J.; Mahmoudi, M. Antibacterial properties of nanoparticles. *Trends Biotechnol.* **2012**, *30*, 499–511. [PubMed]
39. Buzea, C.; Pacheco, I.I.; Robbie, K. Nanomaterials and nanoparticles: Sources and toxicity. *Biointerphases* **2007**, *2*, MR17–MR71.
40. Kuo, W.-S.; Shao, Y.-T.; Huang, K.-S.; Chou, T.-M.; Yang, C.-H. Antimicrobial Amino-Functionalized Nitrogen-Doped Graphene Quantum Dots for Eliminating Multidrug-Resistant Species in Dual-Modality Photodynamic Therapy and Bioimaging under Two-Photon Excitation. *ACS Appl. Mater. Interfaces* **2018**, *10*, 14438–14446. [CrossRef] [PubMed]
41. Yaragalla, S.; Bhavitha, K.B.; Athanassiou, A. A Review on Graphene Based Materials and Their Antimicrobial Properties. *Coatings* **2021**, *11*, 1197. [CrossRef]

42. Ma, Y.; Zhang, M.; Wang, H.; Wang, B.; Huang, H.; Liu, Y.; Kang, Z. N-doped carbon dots derived from leaves with low toxicity via damaging cytomembrane for broad-spectrum antibacterial activity. *Mater. Today Commun.* **2020**, *24*, 101222. [CrossRef]
43. Nichols, F.; Lu, J.E.; Mercado, R.; Rojas-Andrade, M.D.; Ning, S.; Azhar, Z.; Sandhu, J.; Cazares, R.; Saltikov, C.; Chen, S. Antibacterial Activity of Nitrogen-Doped Carbon Dots Enhanced by Atomic Dispersion of Copper. *Langmuir* **2020**, *36*, 11629–11636. [CrossRef]
44. Lin, F.; Li, C.; Chen, Z. Bacteria-Derived Carbon Dots Inhibit Biofilm Formation of *Escherichia coli* without Affecting Cell Growth. *Front. Microbiol.* **2018**, *9*, 259.
45. Santhosh, C.; Kollu, P.; Doshi, S.; Sharma, M.; Bahadur, D.; Vanchinathan, M.T.; Saravanan, P.; Kim, B.-S.; Grace, A.N. Adsorption, photodegradation and antibacterial study of graphene–Fe_3O_4 nanocomposite for multipurpose water purification application. *RSC Adv.* **2014**, *4*, 28300–28308.
46. Jaworski, S.; Wierzbicki, M.; Sawosz, E.; Jung, A.; Gielerak, G.; Biernat, J.; Jaremek, H.; Łojkowski, W.; Woźniak, B.; Wojnarowicz, J.; et al. Graphene Oxide-Based Nanocomposites Decorated with Silver Nanoparticles as an Antibacterial Agent. *Nanoscale Res. Lett.* **2018**, *13*, 116. [CrossRef]
47. Zhu, Z.; Su, M.; Ma, L.; Ma, L.; Liu, D.; Wang, Z. Preparation of graphene oxide-silver nanoparticle nanohybrids with highly antibacterial capability. *Talanta* **2013**, *117*, 449–455.
48. Tang, J.; Chen, Q.; Xu, L.; Zhang, S.; Feng, L.; Cheng, L.; Xu, H.; Liu, Z.; Peng, R. Graphene Oxide–Silver Nanocomposite As a Highly Effective Antibacterial Agent with Species-Specific Mechanisms. *ACS Appl. Mater. Interfaces* **2013**, *5*, 3867–3874.
49. Chang, Y.-N.; Ou, X.-M.; Zeng, G.-M.; Gong, J.-L.; Deng, C.-H.; Jiang, Y.; Liang, J.; Yuan, G.-Q.; Liu, H.-Y.; He, X. Synthesis of magnetic graphene oxide–TiO_2 and their antibacterial properties under solar irradiation. *Appl. Surf. Sci.* **2015**, *343*, 1–10. [CrossRef]
50. Chella, S.; Kollu, P.; Komarala, E.V.P.R.; Doshi, S.; Saranya, M.; Felix, S.; Ramachandran, R.; Saravanan, P.; Koneru, V.L.; Venugopal, V.; et al. Solvothermal synthesis of $MnFe_2O_4$-graphene composite—Investigation of its adsorption and antimicrobial properties. *Appl. Surf. Sci.* **2015**, *327*, 27–36.
51. Kavitha, T.; Gopalan, A.I.; Lee, K.-P.; Park, S.-Y. Glucose sensing, photocatalytic and antibacterial properties of graphene–ZnO nanoparticle hybrids. *Carbon* **2012**, *50*, 2994–3000. [CrossRef]
52. Rajapaksha, P.; Cheeseman, S.; Hombsch, S.; Murdoch, B.J.; Gangadoo, S.; Blanch, E.W.; Truong, Y.; Cozzolino, D.; McConville, C.F.; Crawford, R.J.; et al. Antibacterial Properties of Graphene Oxide–Copper Oxide Nanoparticle Nanocomposites. *ACS Appl. Bio Mater.* **2019**, *2*, 5687–5696. [CrossRef]
53. Yang, Z.; Hao, X.; Chen, S.; Ma, Z.; Wang, W.; Wang, C.; Yue, L.; Sun, H.; Shao, Q.; Murugadoss, V.; et al. Long-term antibacterial stable reduced graphene oxide nanocomposites loaded with cuprous oxide nanoparticles. *J. Colloid Interface Sci.* **2019**, *533*, 13–23. [CrossRef]
54. Liu, S.; Zeng, T.H.; Hofmann, M.; Burcombe, E.; Wei, J.; Jiang, R.; Kong, J.; Chen, Y. Antibacterial Activity of Graphite, Graphite Oxide, Graphene Oxide, and Reduced Graphene Oxide: Membrane and Oxidative Stress. *ACS Nano* **2011**, *5*, 6971–6980. [CrossRef] [PubMed]
55. Akhavan, O.; Ghaderi, E.; Akhavan, A. Size-dependent genotoxicity of graphene nanoplatelets in human stem cells. *Biomaterials* **2012**, *33*, 8017–8025.
56. Akhavan, O.; Ghaderi, E.; Esfandiar, A. Wrapping Bacteria by Graphene Nanosheets for Isolation from Environment, Reactivation by Sonication, and Inactivation by Near-Infrared Irradiation. *J. Phys. Chem. B* **2011**, *115*, 6279–6288. [CrossRef] [PubMed]
57. Rojas-Andrade, M.D.; Chata, G.; Rouholiman, D.; Liu, J.; Saltikov, C.; Chen, S. Antibacterial mechanisms of graphene-based composite nanomaterials. *Nanoscale* **2017**, *9*, 994–1006. [CrossRef]
58. Li, Y.-J.; Harroun, S.G.; Su, Y.-C.; Huang, C.-F.; Unnikrishnan, B.; Lin, H.-J.; Lin, C.-H.; Huang, C.-C. Synthesis of Self-Assembled Spermidine-Carbon Quantum Dots Effective against Multidrug-Resistant Bacteria. *Adv. Healthc. Mater.* **2016**, *5*, 2545–2554. [CrossRef]
59. Hui, L.; Huang, J.; Chen, G.; Zhu, Y.; Yang, L. Antibacterial Property of Graphene Quantum Dots (Both Source Material and Bacterial Shape Matter). *ACS Appl. Mater. Interfaces* **2016**, *8*, 20–25. [CrossRef]
60. Lopez-Diaz, D.; Velazquez, M.M.; Blanco de La Torre, S.; Perez-Pisonero, A.; Trujillano, R.; Garcia Fierro, J.L.; Claramunt, S.; Cirera, A. The role of oxidative debris on graphene oxide films. *Chemphyschem* **2013**, *14*, 4002–4009.
61. Hidalgo, R.S.; López-Díaz, D.; Velázquez, M.M. Graphene Oxide Thin Films: Influence of Chemical Structure and Deposition Methodology. *Langmuir* **2015**, *31*, 2697–2705. [CrossRef]
62. Claramunt, S.; Varea, A.; López-Díaz, D.; Velázquez, M.M.; Cornet, A.; Cirera, A. The Importance of Interbands on the Interpretation of the Raman Spectrum of Graphene Oxide. *J. Phys. Chem. C* **2015**, *119*, 10123–10129. [CrossRef]
63. López-Díaz, D.; López Holgado, M.; García-Fierro, J.L.; Velázquez, M.M. Evolution of the Raman Spectrum with the Chemical Composition of Graphene Oxide. *J. Phys. Chem. C* **2017**, *121*, 20489–20497. [CrossRef]
64. López-Diaz, D.; Merchán, M.D.; Velázquez, M.M. The behavior of graphene oxide trapped at the air water interface. *Adv. Colloid Interface Sci.* **2020**, *286*, 102312.
65. López-Díaz, D.; Solana, A.; García-Fierro, J.L.; Merchán, M.D.; Velázquez, M.M. The role of the chemical composition on the photoluminescence properties of N-doped carbon nanoparticles. *J. Lumin.* **2020**, *219*, 116954.
66. Vera-Agullo, J.; Varela-Rizo, H.; Conesa, J.A.; Almansa, C.; Merino, C.; Martin-Gullon, I. Evidence for growth mechanism and helix-spiral cone structure of stacked-cup carbon nanofibers. *Carbon* **2007**, *45*, 2751–2758. [CrossRef]

67. Peng, J.; Gao, W.; Gupta, B.K.; Liu, Z.; Romero-Aburto, R.; Ge, L.; Song, L.; Alemany, L.B.; Zhan, X.; Gao, G.; et al. Graphene Quantum Dots Derived from Carbon Fibers. *Nano Lett.* **2012**, *12*, 844–849. [CrossRef]
68. Liu, S.; Hu, M.; Zeng, T.H.; Wu, R.; Jiang, R.; Wei, J.; Wang, L.; Kong, J.; Chen, Y. Lateral Dimension-Dependent Antibacterial Activity of Graphene Oxide Sheets. *Langmuir* **2012**, *28*, 12364–12372.
69. Alejo, T.; López-Díaz, D.; Martín-García, B.; Merchán, M.D.; Sánchez-Hidalgo, R.; Velázquez, M.M. 5—Manufacturing ordered films of nanoparticles by Langmuir–Blodgett technique. In *Handbook of Modern Coating Technologies*; Aliofkhazraei, M., Ali, N., Chipara, M., Bensaada Laidani, N., De Hosson, J.T.M., Eds.; Elsevier: Amsterdam, The Netherlands, 2021; pp. 121–138.
70. Velazquez, M.M.; Alejo, T.; Lopez-Diaz, D.; Martin-Garcia, B.; Merchan, M.D. Langmuir-Blodgett Methodology: A Versatile Technique to Build 2D Material Films. In *Two-Dimensional Materials—Synthesis, Characterization and Potential Applications*; InTech: London, UK, 2016; pp. 21–42.
71. Bao, Q.; Zhang, D.; Qi, P. Synthesis and characterization of silver nanoparticle and graphene oxide nanosheet composites as a bactericidal agent for water disinfection. *J. Colloid Interface Sci.* **2011**, *360*, 463–470. [CrossRef]
72. Merchuk, J.C.; Asenjo, J.A. The Monod equation and mass transfer. *Biotechnol. Bioeng.* **1995**, *45*, 91–94. [CrossRef]
73. Tan, Y.; Wang, Z.-X.; Schneider, R.; Marshall, K.C. Modelling microbial growth: A statistical thermodynamic approach. *J. Biotechnol.* **1994**, *32*, 97–106. [CrossRef]
74. Yang, K.; Wan, J.; Zhang, S.; Zhang, Y.; Lee, S.-T.; Liu, Z. In Vivo Pharmacokinetics, Long-Term Biodistribution, and Toxicology of PEGylated Graphene in Mice. *ACS Nano* **2011**, *5*, 516–522. [CrossRef] [PubMed]
75. Dwitya, S.S.; Hsueh, Y.-H.; Wang, S.S.S.; Lin, K.-S. Ultrafine nitrogen-doped graphene quantum dot structure and antibacterial activities against *Bacillus subtilis* 3610. *Mater. Chem. Phys.* **2023**, *295*, 127135. [CrossRef]
76. Tanguy, E.; Kassas, N.; Vitale, N. Protein–Phospholipid Interaction Motifs: A Focus on Phosphatidic Acid. *Biomolecules* **2018**, *8*, 20. [CrossRef] [PubMed]